Polymer Chemistry

Accepted Manuscript

ROYAL SOCIETY OF CHEMISTRY

www.rsc.org/polymers

Journal Name

RSCPublishing

ARTICLE

Tunable Wettability of Hierarchical Structured Coatings Derived from One-Step Synthesized Raspberry-Like Poly(styrene-acrylic acid) Particles

Cite this: DOI: 10.1039/x0xx00000x

Received 00th January 2012,
Accepted 00th January 2012

DOI: 10.1039/x0xx00000x

www.rsc.org/

Xinlong Fan, Xiangkun Jia, Yin Liu, Baoliang Zhang, Chunmei Li, Yali Liu, Hepeng Zhang and Qiuyu Zhang*

A facile one-step method to fabricate hierarchical structured coatings whose wettability could be easily tuned from hydrophilicity (water contact angle, 9.3°) to superhydrophobicity (water contact angle, 154.2°) by controlling the assembly temperature without any specialized equipments or additional modifications is reported. The building blocks for the coatings, hierarchically raspberry-like poly(styrene-acrylic acid) (P(S-AA)) particles with 10 nm corona particles on the core, are produced via a one-step soap-free emulsion polymerization process accompanied by phase separation. The morphology and the roughness of the raspberry-like particles can be conveniently regulated by adjusting the amount of S, AA and divinylbenzene (DVB). The chemical compositions, crosslinking degree, hierarchical structure and roughness of raspberry-like particles have significant influences on the wettability of the coatings. The transition of the wettability is attributed to a thermodynamic-driven process that hydrophobic components of the particles migrate toward the surface of the coatings, and a decrease of the roughness of the hierarchical structure because of the softening and fusing of the particles at the temperature above the Tg of the copolymers.

1. Introduction

Superhydrophobic coatings have been systematically investigated with considerable attention over the past decades. Tremendous progress has been achieved because of their extensively potential applications in the fields of transparent and antireflective superhydrophobic coatings[1-3] for automobile windows, eyeglasses and optical windows for electronic devices, fluidic drag reduction[4, 5], anti-biofouling paints[6-8], suppression of protein and cell adsorption[9, 10], water-oil separation[11-13], superhydrophobic textiles[14-16] and synthesis of particles[17, 18]. Strategies commonly used to obtain superhydrophobicity are producing rough surfaces with hierarchical structure and lowering surface energy according to the theoretical research based on the work of Wenzel[19] and Cassie[20]. In view of the concrete methods for fabricating superhydrophobic surfaces, lithography[21-23], templating[24-26], plasma treatment[27-29], chemical vapor deposition[30-32], layer-by-layer (LBL) deposition[33-35], phase separation[36-38], electrospinning[39-41] and colloidal assembly[42-44] have been developed.

Among the aforementioned methods, lithography, preparing superhydrophobic surface by copying desired features from a master and then transferring it to a replica in an opposite form, is a very useful method for fabricating rough surfaces with regular structures. However, this top-down lithographic method is a time-consuming technology suffering from low throughput and high cost, and is only suitable for small areas. For this reason it has mostly been applied to produce surfaces for fundamental research of superhydrophobicity[45]. Templating that involves the replication of desired features from a master by molding and subsequently lifting off the replica or dissolution of the template is often useful for the preparation of polymeric superhydrophobic coatings. The templating processes should be handled with care to avoid damaging both the replica and the template, thus it might not be fit to fabricate irregular surface patterns with excessively complex structures[46]. Plasma treatment is an efficient method that could provide the as-prepared materials with surface roughness and low surface energy simultaneously, while the high efficient method with a total processing time of a few minutes is less controllable[47]. The chemical deposition including chemical vapor deposition and LBL deposition is a process by exposing the selected substrate to a gaseous precursor or polyelectrolyte to deposit the desired film. Nevertheless, due to the relatively extensive operation procedures, the chemical vapor deposition method fails to precisely control the detail at each individual spot of the surface. And the LBL deposition is also difficult to precisely control the surface patterns because nanoparticles, mostly silica particles, are often added into the deposition to achieve the surface roughness. Structures obtained from phase separation usually have microscale papillae, while the nanoscale papillae papared by this method are more prone to collapse during the process of drying. The electrospinning technique is a versatile method for manufacturing nanomaterials with controllable compositions and structures, which therefore provides an ideal strategy for construction of superhydrophobic surfaces[48].

Most of the discussed methods for preparing superhydrophobic coatings necessarily need expensive materials (e.g. perfluoroalkyl silane, nanotubes), complicated production equipments or operation procedures. The potential for industrial applications requires surfaces to be reproducible and low cost and to be processed rapidly. Colloidal assembly method, in which the surface roughness and surface energy could be easily tuned by controlling the morphology and size of colloids and treating with low surface energy materials including long alkyl chain thiols, fatty acids and organic silanes, is

comparatively more economical. It can be applied to fairly large surface areas with ordered or non-ordered roughness on scale from nanometer to micrometer and does not require any specialised equipment. Raspberry-like colloidal particles are one of the most promising building blocks for colloidal assembly method to construct superhydrophobic coating[49, 50] because of their unique hierarchical structure, designed surface properties and higher surface roughness compared with smooth particles. Among these characteristics, hierarchical structure receives the most attention since that theoretical analysis and numerous experimental studies have proved that multiscale roughness consisting of nanometer sized papillae on top of micrometer sized protrusions plays a vital role in realization of superhydrophobic surface[51-53]. In most cases, hierarchical structured raspberry-like particles with nanoscale silica or titania attached to submicron or micron particles were used to assemble superhydrophobic coatings. Surfaces of the raspberry-like particles were commonly fluorinated or functionalized with silane or long chain alkane to reduce surface energy, which increased the cost and made the procedure for producing raspberry-like particles a multi-step process. Actually, raspberry-like particles were rarely prepared via a simple one-step process.

In order to reduce the cost of fabricating superhydrophobic coatings and achieve industrialization, some research groups have proved that fluoride-free, silane-free and long-alkyl-chain-free materials with low cost and polystyrene or polymethylmethacrylate contained could be used to fabricate superhydrophobic coatings by templating[26], phase separation[37] and electrospinning[39]. To overcome the disadvantages of current approaches to low cost superhydrophobic coatings, Wang et al[54, 55] reported that smooth poly(styrene-n-butyl acrylate-acrylic acid) and poly(styrene-block-methyl methacrylate-block-acrylic acid) core-shell particles prepared by soap-free emulsion polymerization showed tunable wettability from superhydrophilic to superhydrophobic by changing the assembly temperatures. However, up to now, there is no report about one-step assembly of superhydrophobic coatings from hierarchical structured raspberry-like particles that were produced with fluoride-free, silane-free and long-alkyl-chain-free materials.

Herein, inspired by our previous work[56], we report a simple one-step synthesis of monodisperse raspberry-like polymer particles using soap-free emulsion polymerization of styrene (S) and acrylic acid (AA). In this method, when S, AA and potassium persulfate (KPS) were mixed with water and stirred at a certain temperature for a period of time, hierarchical structured raspberry-like P(S-AA) particles with nanosized corona particles on the large core particles were produced. Hierarchical structured coatings assembled from these one-step synthesized raspberry-like particles without any specialized equipments or additional modifications showed tunable wettability that could be tuned from hydrophilicity (water contact angle, 9.3°) to superhydrophobicity (water contact angle, 154.2°) by controlling the assembly temperature. The hierarchical structure of the coatings as well as the migration of hydrophobic components during the assembly process is the key factors of the transition of wettability.

2. Experimental Section

2.1. Materials. Styrene (S, 99.5%, J&K Scientific Ltd.), Acrylic acid (AA, 99.5%, Sinopharm Chemical Reagent Co., Ltd.) and divinylbenzene (DVB, ≥80%, Tokyo Chemical Industry Co., Ltd.) were purified by distilling under reduced pressure and stored in a refrigerator prior to use. Potassium persulfate (KPS, 99%, Sinopharm Chemical Reagent Co., Ltd.) was purified by recrystallization from water. Other reagents from Sinopharm Chemical Reagent Co., Ltd. were used directly as received without further purification. Ultrapure water was used throughout the whole experiment.

2.2. Preparation of Raspberry-Like P(S-AA) Particles. Monodisperse P(S-AA) particles were prepared by soap-free emulsion polymerization. The detailed experimental conditions in this paper and pH and zeta potential of the final P(S-AA) colloidal suspensions without any post-processing were listed in Table S1. Typically, a total amount of 3g monomers and water (80 mL) were added into a three-neck round-bottomed flask equipped with a paddle agitator and reflux condenser. The mixture was stirred at a speed of 200 rpm and heated to 80 °C. Then KPS (0.07 g in 20 mL water) was added and stirred for 12 h to produce P(S-AA) particles.

2.3. Assembly of Hierarchical Structured Coatings. Prior to use glass slide with a size of 20×20 mm^2 was treated in a piranha solution (a mixture containing 98% concentrated sulfuric acid and 30% hydrogen peroxide in a volume ratio of 7:3) at 80 °C for 2 h and rinsed thoroughly with water to remove any contaminant. (Warning: The piranha solution reacts violently with organic materials. Handle with caution.) The obtained colloidal suspensions containing nearly 3 wt% raspberry-like particles without any purification were diluted with seventeen fold water to 0.17 wt%. A glass slide was vertically immersed into the diluted P(S-AA) colloidal suspensions in a vial. Then the vial was vertically placed in a constant temperature chamber at temperatures of 25, 40, 50, 60, 70, 80, 90, 100, 110 and 120 °C. Depending on the different assembly temperature, it took less than 10 h (at 120 °C) to 7 days (at 25 °C) to completely vaporize water in the suspensions. The coatings were obtained when water evaporated, leaving particles deposited on the glass slides.

2.4. Characterization. Particle size distribution of P(S-AA) particles dispersed in water was determined by laser particle analyzer (LS13320, Beckman Coulter Instruments). The pH of the soap-free emulsion system was measured by a pH meter (PHS-3C, Shanghai REX Instrument Factory) at room temperature. The zeta potential of the P(S-AA) colloidal suspensions was assayed using a Beckman Coulter Delsa™ Nano C particle analyzer. A scanning electron microscopy (SEM, JSM 6700F, JEOL, Japan) was employed to observe the morphology of the resulting product; Particles in suspensions were deposited onto a clean silicon wafer, samples on silicon wafer and coatings on glass sildes were sputtered with platinum by a JFC-1600 auto fine coater at a current of 20 mA for 180 s before examination. TEM observations of P(S-AA) particles were conducted on a JEM 2010 transmission electron microscopy (JEOL, Japan) at an accelerating voltage of 200 kV. The sample for TEM observations was prepared by placing diluted particles on a copper grid. The water evaporated at room temperature, leaving the solid aggregates on the copper grid. Coatings on the glass slides were peeled off and then placed on a copper grid. Samples for slice TEM were embedded into low-viscosity epoxy resin and cured before cryo-microtoming into 50~70 nm thick slices. These slices were collected on TEM grids. TEM experiments were performed on a JEM 2010 at 120 kV with an emission current as low as 3 μA and minimal exposure time to minimize electron-beam-induced morphological changes and damages. Elemental composition of P(S-AA) particles was analyzed on an elemental analyzer (Vario EL III, Elementar Analysensysteme GmbH) with CHN mode. The images of water contact angles were recorded with an ultrapure water droplet of 8 μL on a JC2000D1 contact angle analizer (Powereach, China) at room temperature. All the contact angle values were determined by averaging values measured at least five different points on each sample surface using Laplace-Young fitting mode. Glass transition temperature (Tg) of the particles was performed in argon atmosphere using a differential scanning calorimeter (DSC823e, Mettler Toledo) at a heating rate of 10 °C/min. In order

to remove unpolymerized monomers and soluble PAA in colloidal suspensions, all the particle suspensions used for testing on SEM, TEM, elemental analyzer and DSC were washed with methanol and water for 3 times by high speed centrifuge, respectively. X-Ray photoelectron spectroscopy (XPS) data measured at a 90° takeoff angle were obtained with an AXIS Ultra DLD spectrometer (Kratos Analytical Co. Ltd., UK) equipped with a 300 W monochromatic Al Kα X-Ray source. The binding energies were referenced to the C1s line at 284.7 eV from adventitious carbon. Atomic force microscopy (AFM) images were recorded using an instrument SPI3800-SPA-400 (Japan, NSK Ltd.) atomic force microscopy in tapping mode equipped with Olympus cantilevers.

3. Results and Discussion

3.1. Morphology Development of P(S-AA) Particles

P(S-AA) particles with smooth strctures have been extensively fabricated by soap-free emulsion polymerization for various purposes in the past decades[57-61]. In previous work, AA was only used as a minority monomer to introduce carboxyl group to the particles in order to improve the hydrophilicity and stability. To the best of our knowledge, up to the present, particles with rough surface have not been prepared by the copolymerization of S and AA, probably because that the amount of AA in the recipe was not big enough. In this paper, P(S-AA) particles were prepared by soap-free emulsion polymerization with different monomer mole ratios. The pH value and the zeta potential of the colloidal suspensions are present in Table S1. The pH values of all the final suspensions are around 2.4, which mainly resulted from hydrogen ion produced by the decomposition of KPS. Sulphonic groups at the end of the polymer chains and carboxyl groups attributed to AA on the surfaces endow the particles with large zeta potential (< -40 mV), generating a very stable colloidal suspension. Size distributions of P(S-AA) particles prepared at different condtions shown in Fig. S1-S3 indicate monodisperse colloidal particles can be produced by this method.

Fig. 1 shows TEM and SEM images of the as-obtained P(S-AA) particles as a function of the initial monomer mole ratio of S and AA. The morphologies of the P(S−AA) particles were significantly influenced by the monomer ratios. When the mole ratio of S/AA was 80/20, smooth and homogeneous structures were obtained (Fig. 1a), which were very similar to the structures reported by previous papers. By increasing the mole fraction of AA in the monomers, the particles became rough and hetergeneous, some nanosized corona particles around 10 nm were anchored on the surface of core particles, forming hierarchical structured raspberry-like particles (Fig. 1b). When the mole fraction of AA was increased to 50% and 60%, particles showed rough structures similar to the case of 40% AA mole fraction. While particles with flower-like structures were obtained by further increasing the amount of AA (Fig. 1e).

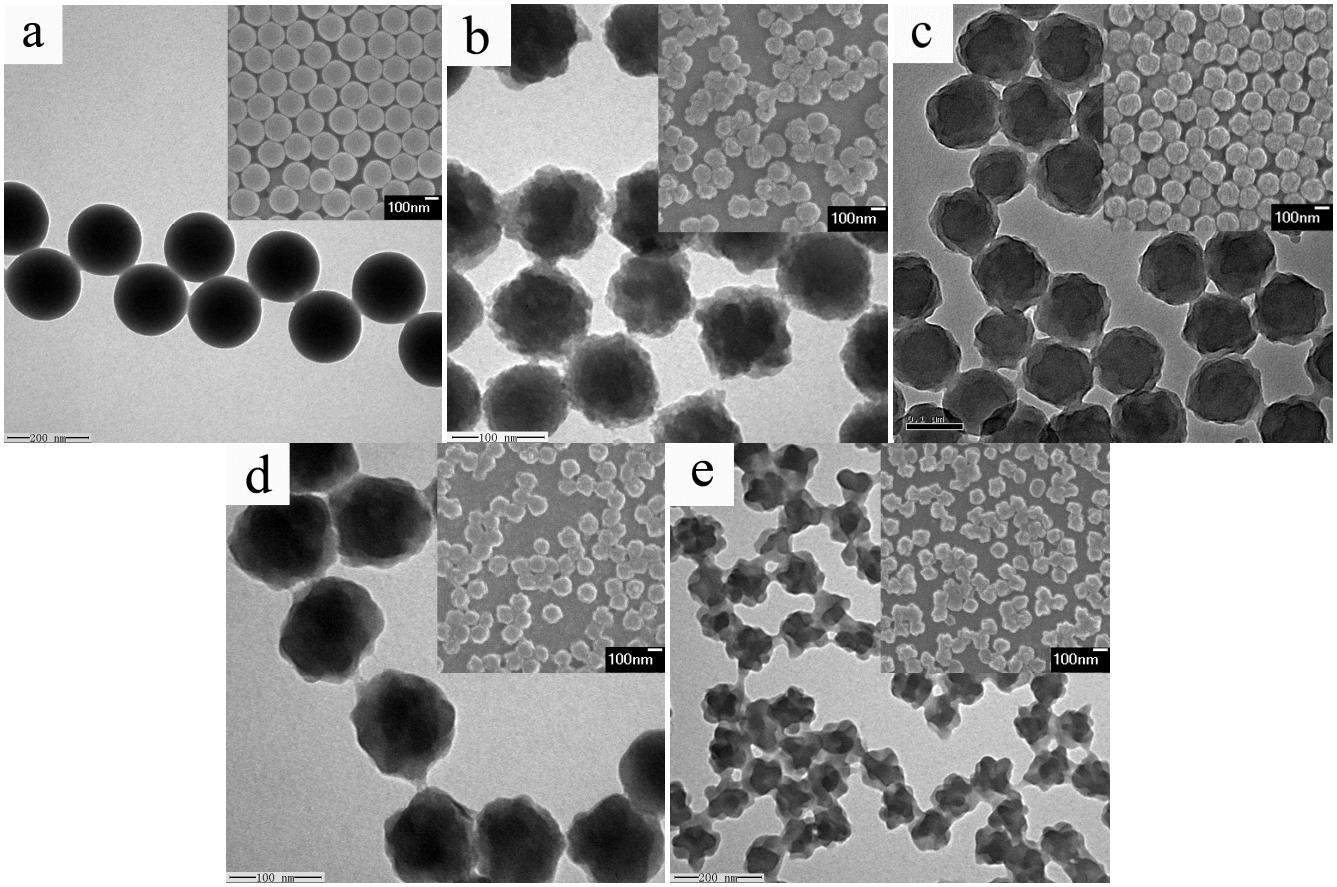

Fig. 1 TEM and SEM images of P(S-AA) particles prepared with different monomer mole ratios, (a) S/AA=80/20; (b) S/AA=60/40; (c) S/AA=50/50; (d) S/AA=40/60; (e) S/AA=20/80.

Variation of morphologies in Fig. 1 indicated that the initial monomer composition was the key factor to influence the formation of particles with various structures. When AA was added to the soap-free emulsion copolymerization system, similar to previous reports[57-61], AA was more likely to polymerize than S because of its high water solubility. Even so, S could also participate in the polymerization to some extent since that minority S was dissolved in water. Based on the theory of homogeneous nucleation, as the

oligomer radicals propagated to a critical length, they precipitated and agglomerated to form primary particles. Then monomers began to enter the primary latex particles and swell the copolymers, and copolymers growth continued inside the particles. The carboxyl groups attached to the copolymers concentrated at the particles/water interface to form a thin hydrophilic shell and maintain their stability. When the mole fraction of AA was 20%, most of the AA depleted in the early stage of the polymerization to form relatively hydrophilic primary particles, Most S and possibly tiny amount of AA were left to swell the primary particles. Thus polymers formed in the primary particles rapidly turned from hydrophilic to relatively hydrophobic, residual S was more prone to swell these hydrophobic polymers and polymerize in the hydrophobic environment. The final S-enriched polymers aggregated in the interior of the particles to form hydrophobic core and no distinct phase separated structures were observed mostly because of relatively smaller amount of hydrophilic AA-enriched copolymers. When the mole fraction of AA was increased, the amount of AA-enriched copolymers participated to produce primary particles in the early stage of the polymerization increased as well. Residual AA swelled in the particles depleted faster than S swelled in the particles since the reactivity ratios of S and AA were 0.15 and 0.25[62, 63]. After AA was totally depleted residual S swelled in the particles continued to polymerize to form hydrophobic S-enriched copolymers. Thus, the S-enriched copolymers were crushed into the interior of particles because of their hydrophobicity and formed domains[64]. Large amount of AA-enriched copolymers migrated toward the surfaces of the polymer particles as more S monomer involved in polymerization inside the latex particles. Because the transfer of AA-enriched segments toward the surfaces of particles was driven by phase separation, these segments could not form uniform shells but rather corona around the particle surfaces[65]. The distributions of S-enriched and AA-enriched copolymers were demonstrated by TEM image of slices of P(S-AA) particles prepared with S/AA=50/50 (Fig. S4), in the image particles possessed higher contrast in the central regions than peripheral regions. The higher contrast regions were attributed to S-enriched polymers, which was because that benzene rings in the S-enriched polymers had higher electron density than AA-enriched polymers and epoxy resin around the particles.

As the AA mole fraction increased, the AA-dominated polymers formed in the early stage of the polymerization might not precipitate because of their strong hydrophilicity unless the hydrophobic constituents in the copolymers increased to a critical value. This was the reason why the mass fractions of AA in the ultimate P(S-AA) particles (Fig. S5) calculated from the data of elemental compositions (Table S2) were much lower than that in the original monomer mixtures. When the AA mole fraction was 80%, there were maybe an increasing number of strong hydrophilic polymers that would not precipitate to form the primary particles, resulting in a little smaller of the size of corresponding P(S-AA) particles (Fig. S1).

There was a very obvious increment of the surface roughness when crosslinker was added into the polymerization. Fig. 2 shows the TEM and SEM images of P(S-AA) particles with 6% mole fraction of DVB. Compared with Fig. 1, many more corona particles with a size around 10 nm were emerged on the core particles (Fig. 2), which made the surface of the hierarchical structured particles much rougher. It was noteworthy that the particles obtained with monomer ratio of S/AA/DVB=75.2/18.8/6 (Fig. 2d) were no longer smooth even though the particles with the same S/AA monomer ratio but without crosslinker showed homogeneous structures (Fig. 1a).

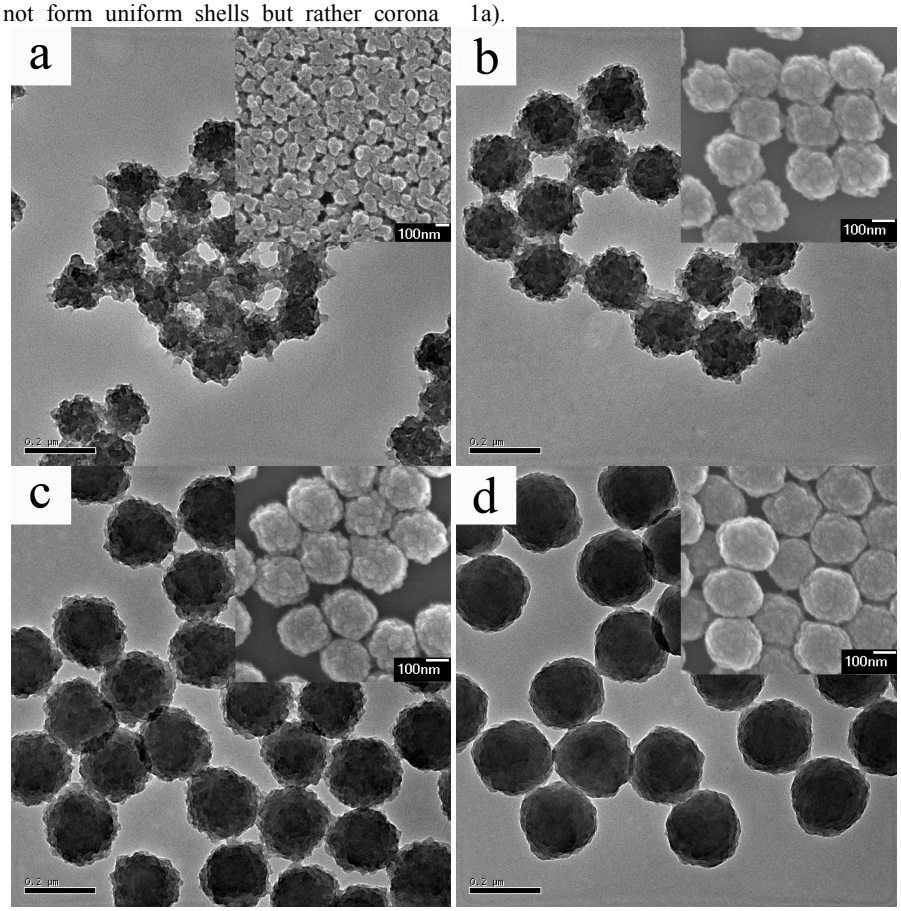

Fig. 2 TEM and SEM images of P(S-AA) particles prepared with 6% DVB mole ratio but different S and AA ratios, (a) S/AA/DVB=18.8/75.2/6; (b) S/AA/DVB=37.6/56.4/6; (c) S/AA/DVB=56.4/37.6/6; (d) S/AA/DVB=75.2/18.8/6.

Compared with S and AA, DVB with two reactive double bonds was more active. DVB could accelerate the process of nucleation, leading to a decrease of the amount of strong hydrophilic polymers that did not prepcipitate. This was demonstrated by a higher amount of mass fraction of AA in the ultimate crosslinked P(S-AA) particles (Fig. S6) than that of noncrosslinked particles, the mass fractions of AA in the particles were also calculated from the data of elemental compositions (Table S3).When residual monomers swelled in the particles continued to polymerize, the copolymers produced in the later stage of the polymerization were hydrophobic and crushed into the interior of particles. Owing to the increasing of the amount of hydrophilic copolymers by the introduction of crosslinker, there was an increasement of AA-enriched copolymers that could participate in the phase separation process, leading to more distinct phase separated structures (Fig. 2d).

TEM and SEM images in Fig. 3 show the morphologies of raspberry-like P(S-AA) particles with the same S/AA mole ratio but different DVB contents. Comparing the structures in Fig. 1c with Fig. 3a-b, it was found that crosslinked particles possessed rougher surfaces when the DVB content was increased, which could be explained by the increasement of the content of AA in the ultimate particles as the increase of crosslinking degree (Fig. S7, data in which were calculated from Table S4). However, by further increasing the DVB content to 6% and 8%, the degree of phase separation was not enhanced comparing with the case of 4% DVB. It may be because that more crosslinker restricted the migration of AA-enriched polymers toward the surfaces, even though the amount of AA-enriched copolymers was increased.

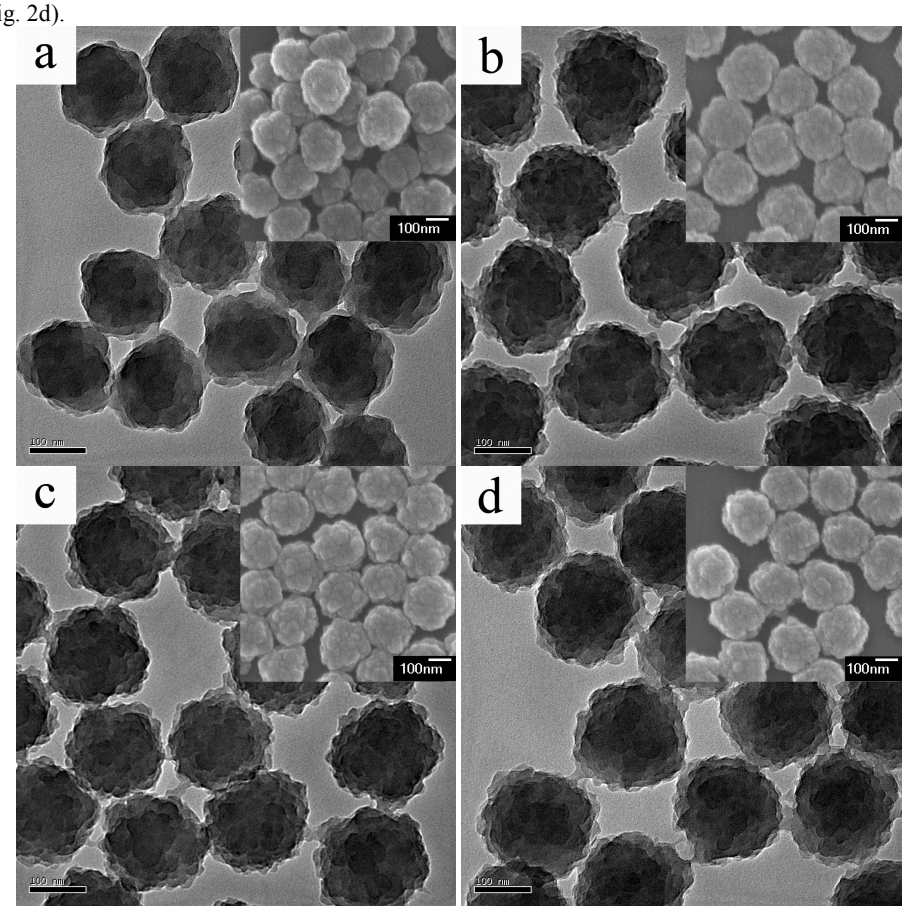

Fig. 3 TEM and SEM images of P(S-AA) particles with prepared different DVB mole ratios, (a) S/AA/DVB=49/49/2; (b) S/AA/DVB=48/48/4; (c) S/AA/DVB=47/47/6; (d) S/AA/DVB=46/46/8.

In brief summary, hierarchical structured raspberry-like P(S-AA) particles with different morphologies were produced via a one-step soap-free emulsion polymerization. The regularity of the corona particles and the roughness of the raspberry-like particles can be easily controlled by altering the mole ratio of S/AA and the amount of DVB.

3.2. Wettability of Coatings Assembly from Raspberry-Like P(S-AA) Particles

Based on the as-prepared hierarchical structured raspberry-like P(S-AA) particles with various morphologies, coatings assembly from P(S-AA) particles were fabricated via a vertical deposition method at temperatures of 25, 40, 50, 60, 70, 80, 90, 100, 110 and 120 ^{o}C. Although Coatings with different thicknesses could be produced by controlling over the parameters of vertical deposition method[66, 67], investigation of the effect of thickness on the wettability of the coatings was out of the scope of this paper. Water contact angles of the coatings assembly from particles with different mole ratios are presented in Fig. 4. It can be seen that the coatings produced with different particles at different temperatures showed different wettabilities. The wettability of the coatings can be altered from hydrophilic to superhydrophobic by controlling the assembly temperature. The coatings fabricated at room temperature were hydrophilic with contact angles around 20^{o}. The contact angles of the coatings produced with different particles at room temperature initially decreased as the decrease of AA mole fraction in the particles and showed a minimum value of 16.8^{o}, then slightly increased to 22.8^{o} by further decreasing the AA mole fraction. The contact angles of the coatings rapidly increased by increasing the assembly temperature until the temperature was above 100 ^{o}C. All of the coatings became hydrophobic when the tempreture increased to 60 ^{o}C. Especially, the coatings assembly from the particles prepared with the initial monomer ratio of S/AA=60/40 reached a

superhydrophobic state (152.3°) when the assembly temperature was 90 °C, and increased to 154.2° at 100 °C. However, all the contact angles decreased by further increasing the assembly temperature to 110 and 120 °C. At high assembly temperature, the contact angles of the coatings fabricated at same temperature increased as the decrease of AA mole fraction in the particles and showed maximum value when the particles were produced with the initial monomer ratio of S/AA=60/40, while the contact angles of coatings assembly from the particles prepared with the initial monomer ratio of S/AA=80/20 were much smaller than the case of S/AA=60/40. Fig. S8 shows the advancing contact angles, receding contact angles and contact angles hysteresises (CAH) of the coatings assembly from the particles prepared with 60% S and 40% AA. Considerable CAH values varied from 46 to 55° were observed when the coatings were assembled at relatively high temperatures, and water droplets could hardly roll off the coatings, showing high adhesion similar to petals' surfaces of red roses[68].

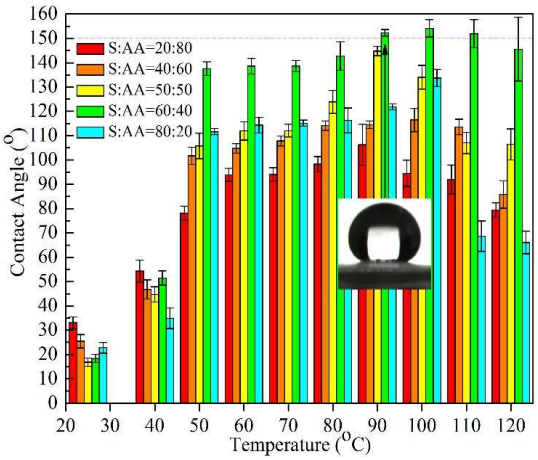

Fig. 4 The relationships of fabrication temperatures and contact angles of the coatings assembly from particles with various composition ratios.

Numerous researches have proved that the wettability of a surface is mainly dominated by chemical constituents and roughness of the surface structures, low surface energy chemicals could improve the hydrophobicity, while the roughness could make a hydrophilic surface more hydrophilic and a hydrophobic surface more hydrophobic[45, 46]. Changes of the contact angles of the coatings produced with different particles at same temperature were mainly attributed to the difference in the roughness of the coatings that resulted from the hierarchical structures of the building blocks. TEM images in Fig. 1 have already confirmed that the roughness of the particles increased as the increase of S content in the particles until the mole fraction of S in the initial monomer mixtures became 60%. Although in the case of 20% S mole fraction, the particles obtained showed rougher surfaces in TEM images because of its flower-like structure, the contact angles of the coatings assembly from the corresponding particles were higher than any other coatings fabricated at room temperature, and lower at high temperature. It may be because that the particles with large amount of AA shrinked more severely in the absent of water than particles with less AA, which could be seen in the SEM image inserted in Fig. 1e. The shrink of the particles in dry state reduced the surface roughness. Therefore, the wettabilities of the coatings were improved at room temperature and got worse at high temperature as the increase of S content in the particles in the range of ≤ 60% mole fraction of S. The smooth and homogeneous structures of the particles derived from the recipe of 80% S and 20% AA should be responsible for that the contact angle of the coatings assembly from which was higher at room temperature and much lower at high temperature than the coatings assembly from the hierarchical structured particles prepared with 60% S and 40% AA.

The coatings assembly from the particles prepared with 60% S and 40% AA were extracted to study the wettability change of the coatings fabricated at different temperatures. SEM images of the coatings fabricated at different temperatures are shown in Fig. 5 and Fig. S9. The particles were regularly arranged to form hexagonally packed ordered structures with hierarchical surfaces. The raspberry-like particles themselves formed submicro scale roughness, while the corona particles on the core particles formed nano scale roughness. From the SEM images we can see that coatings fabricated at the temperature ranged from 25 to 100 °C had very similar morphology, no obvious change of the hierarchical structures was observed. However, when the assembly temperature was increased to 110 °C and above the Tg of P(S-AA) (Fig. S10), the particles softened and fused with each other to produce relatively smoother surface, which was a typical process for latex film formation[69]. By comparing the TEM images of the coatings (Fig. 6) assembly at 100 °C (Fig. 6a) and 120 °C (Fig. 6b), it was found that the building blocks of the coatings still had rough structures and could be distinguished from each other at 100 °C. However, they fused and no individual particle could be found when the assembly temperature was 120 °C. Thus the hierarchical structures with nanosized corona particles on the surface of submicrosized particles were damaged, which casued reduction of the roughness of the coatings and decreased the apparent hydrophobicity. Fig. S11 shows typical 3-dimensional AFM image, height image and cross-sectional profile of the coatings assembly from the particles prepared with 60% S and 40% AA at room temperature. The roughness factors of the coatings fabricated at different temperatures were measured by AFM and showen in Fig. S12. The roughness factor which was referred to as the roughness area ratio of the actual surface with respect to the geometric surface irregularly ranged from 1.13 to 1.17 when the assembly temperature was below 110 °C, the small variation of which was believed to be the measure error. While the roughness of the coatings decreased as the temperature increased to 110 and 120 °C. So far, it could be speculated that the decrease of the contact angles of the coatings at 110 and 120 °C was probably owing to the decrease of the roughness. While both SEM and AFM data revealed that there was no significant change in the roughness and hierarchical structure of the coatings when the assembly temperature was below 110 °C, This indicated that the transition of wettability of the coatings fabricated at different temperatures were not merely caused by the alteration of surface roughness.

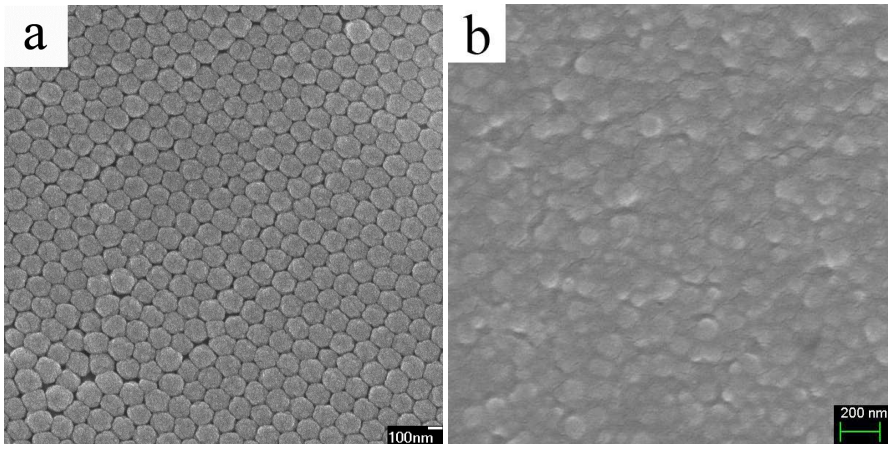

Fig. 5 SEM images of the coatings assembly from particles prepared with 60% S and 40% AA fabricated at (a) 25 and (b) 120 °C.

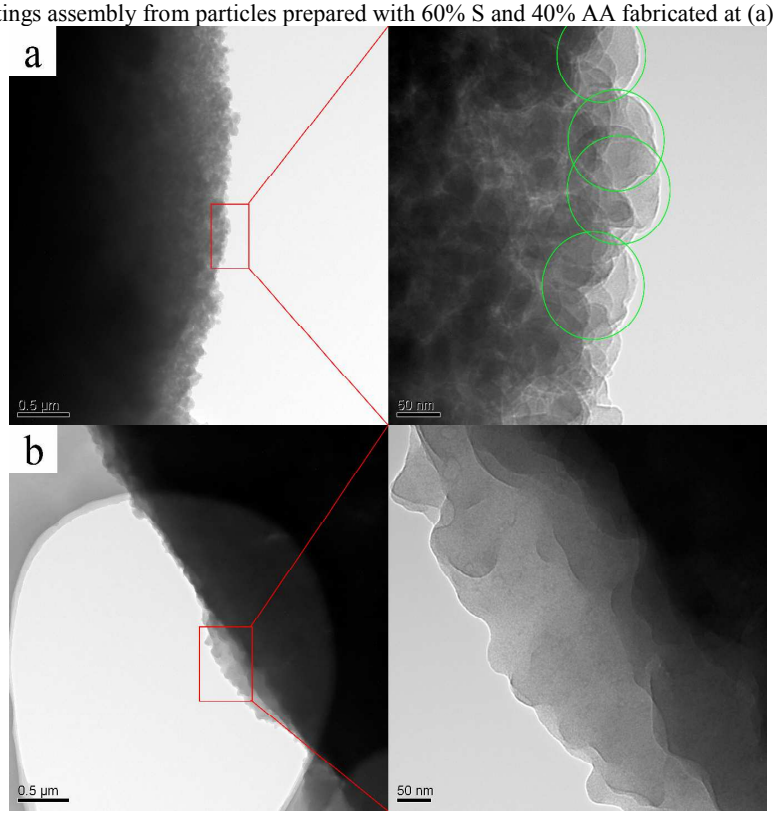

Fig. 6 TEM images of the coatings assembly from particles prepared with 60% S and 40% AA fabricated at (a) 100 and (b) 120 °C.

Since there was no significant change in the hierarchical structure of the coatings when the temperature was below 110 °C, alteration of chemical composition would probably be the reason of the transition of wettability. XPS was used to clarify the change of chemical component of the surface. Fig. 7 and Fig. S13 show the X-Ray photoelectron spectra of the coatings assembly from the particles prepared with 60% S and 40% AA at different temperatures. Fig. 7a is a wide X-Ray photoelectron spectrum of coatings fabricated at room temperature. The only two peaks at 285 eV and 529 eV attributed to carbon 1s and oxygen 1s proved that there were only three elements including carbon, hydrogen and oxygen existed on the surface on the coatings. Fig. 7b, Fig. S13 and Fig. 7c are the high resolution XPS peaks of carbon 1s of the coatings assembly at room temperature, 40, 50, 60, 70, 80, 90, 100, 110 and 120 °C, respectively. In the broad carbon peak, four different components were found at 284.7, 285.5, 289.5 and 291.4 eV, which corresponded to the functional groups of C-H/C-C, C-O, C(O)O and the $\pi^* \leftarrow \pi$ shakeup of benzene ring, respectively. The existence of shakeup peak in the XPS of the coatings fabricated at room temperature indicated that certain amount of PS constitutent was on the surface of the particles. The intensity of the C-O peaks attributed to PAA constitutent gradually decreased as the increase of assembly temperature, while the intensity of the C-H/C-C peaks attributed to hydrophobic components relatively increased as the increase of the assembly temperature (Fig. 7d) regardless of the temperature above or below the Tg of P(S-AA).

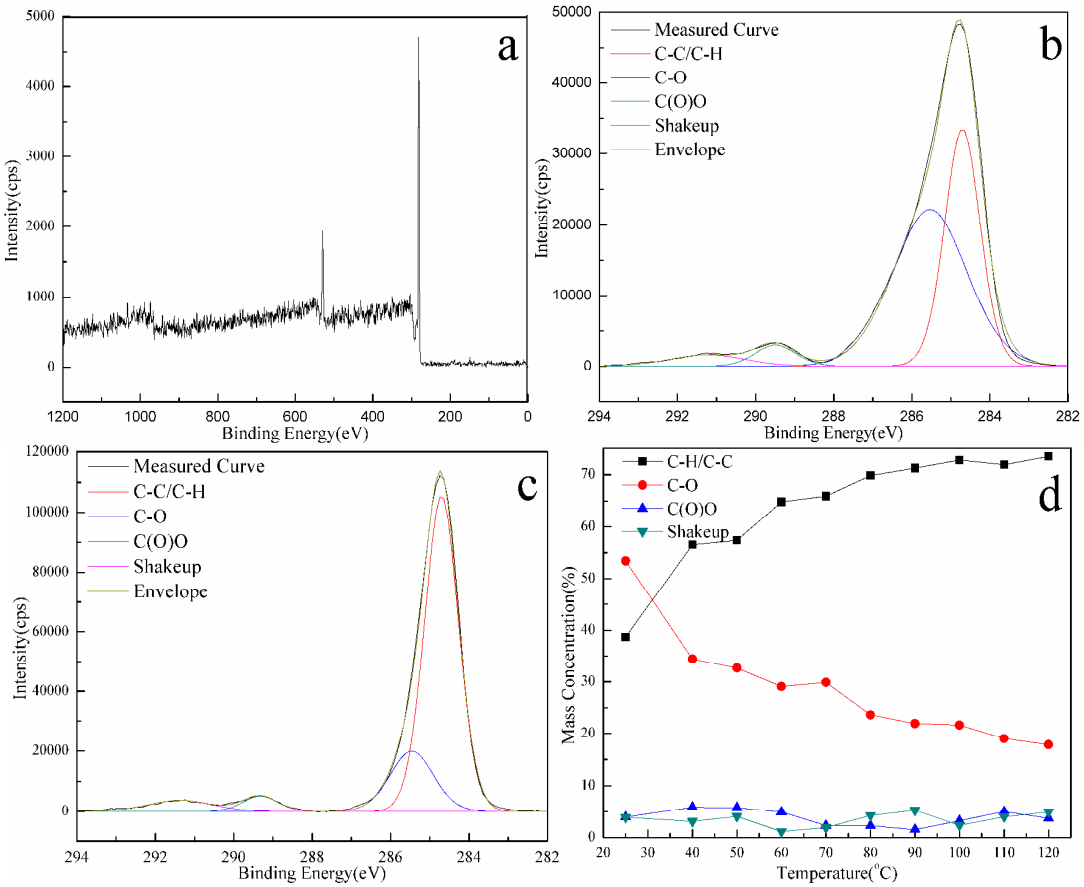

Fig. 7 XPS results of the coatings assembly from particles prepared with 60% S and 40% AA: (a) wide spectra of coatings fabricated at 25 °C and high resolution spectral peaks of carbons at (b) 25 and (c) 120 °C, and (d) the variation of the content of carbons attributed to different groups at different temperatures.

The changes of the intensity of C-O and C-H/C-C peaks confirmed that the hydrophobic components migrated to the surface of the particles as the increase of the assembly temperature, which was consistent with the research of Wang et al[55]. During the process of the coating formation, as water in the suspension evaporated and particles was deposited on the glass slide, the polar water around the particles was replaced by apolar air. The hydrophilic carboxyl and sulfate groups were inclined to evade the apolar air and migrate toward the interior of the particles, while hydrophobic components preferred to migrate toward the apolar air[70]. At a temperature below the Tg, the motion of carboxyl and phenyl groups on the side chains of polymers and the Schatzki crankshaft motion of the main chain on the surface of the particles could happen if they were given enough energy to overcome energy barrier. Therefore, at a low temperature such as room temperature, the motion of the side chain and main chain was blocked by the energy barrier, and there were abundant carboxyl groups on the surface as proved by XPS data (Fig. 7b). As the temperature increased, enough energy was obtain to initiate the motion of the carboxyl groups toward the interior of the particles and the motion of phenyl and main chain toward the surface of the particles, resulting in a decrease of C-O and increase of C-C and C-H (Fig. 7d). It is worth noting that even at high temperature, there were still about 20% hydrophilic C-O attributed to carboxyl groups on the surface of the coatings, which allowed the droplets to partially penetrate into the hierarchical structure of the coatings, leading to a high CAH and high adhesion.

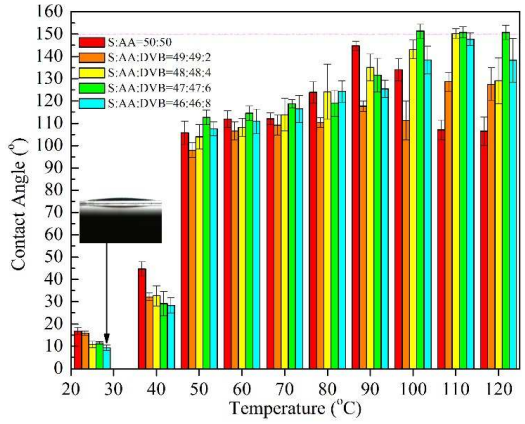

Fig. 8 The relationships of fabrication temperatures and contact angles of the coatings assembly from particles with various crosslinking degrees.

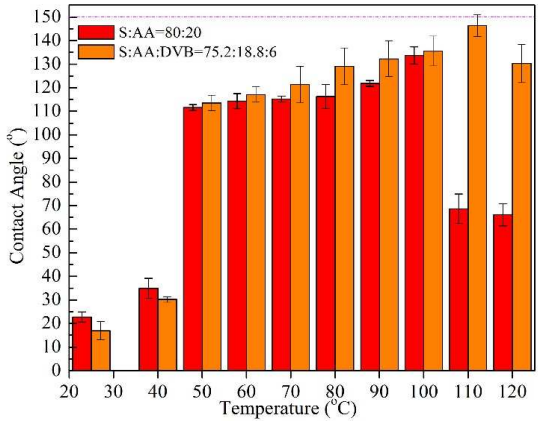

Fig. 9 The relationships of fabrication temperatures and contact angles of the coatings assembly from particles with various surface roughness.

Contact angles of the coatings assembly from raspberry-like particles with different crosslinking degrees were also measured and presented in Fig. 8. The contact angles of the coatings decreased as the increase of crosslinking degree at room temperature, this was mainly because of the increase of roughness of the surface as the increase of crosslinking degree. When the crosslinking degree was increased to 8%, the contact angle of the corresponding coating was 9.3°, which was the lowest value obtained in this paper. The contact angles of the coatings increased as the increase of the fabrication temperatures. However, at the same temperature below 100 °C, there was no obvious relationship between the contact angles and the crosslinking degree. The contact angle of the coatings assembly from crosslinked particles only became distinctly higher than that from noncrosslinked particles when the temperature was increased to 100 °C, which was probably because that the crosslinked coatings had higher Tg and could maintain the hierarchical structures. The contact angles of the coatings with 4% and 6% crosslinking degree increased above 150° when the temperature reached 100 and 110 °C. Similar to the coatings without crosslinker, there was a slightly decrease of the contact angles of the crosslinked coatings when the temperature increased to 120 °C, the difference was that the degree of reduction was much smaller. Although it was beneficial for the enhancement of hydrophobicity of the coatings by increasing the surface roughness via the introduction of crosslinker into the polymerization, crosslinker in the particles could also restrict the migration of the hydrophobic groups in the copolymers toward the surface of the particles. Hence, the introduction of crosslinker into the copolymers was a double-edged sword to the hydrophobicity of the coatings. On one hand, the crosslinker could increase the roughness of the coatings, enhance the resistance to deformation and strengthen the hydrophobicity, on the other hand, the crosslinker could also restrict the migration of the groups and decrease the hydrophobicity. It depended on that which of the two effects dominated in a specific condition. As for the coatings assembly from the relative rougher particles prepared with 75.2% S, 18.8% AA and 6% DVB, the contact angles of that were a bit larger than the contact angles of the coatings assembly from the smooth particles prepared with 80% S and 20% AA (Fig. 9). The morphologies of the coatings were characterized by SEM and shown in Fig. S14. In this case, the enhancement of hydrophobicity resulted from the increase of roughness prevailed over the decrease of hydrophobicity resulted from the restriction of the migration of hydrophobic components by crosslinking.

On the basis of these results, we proposed a possible mechanism of the wettability change of the hierarchical structured coatings assembly from raspberry-like P(S−AA) particles at different temperatures, as shown in Scheme 1. At room temperature, the coatings showed hydrophilicity because that hierarchical structure of the raspberry-like particles increased the surface roughness of the coatings and enhanced the hydrophilicity caused by the strong hydrophilic groups on the surface of the coatings. At an elevated temperature, the side chain groups and main chains received enough energy to overcome the energy barrier. The hydrophilic groups including carboxyl and sulfate migrated to the interior of the particles in order to evade the apolar air around the coatings, and the hydrophobic groups including phenyl on the side chain and methylene on the main chain migrated toward the surface. The thermodynamic-driven movement of the groups decreased the surface energy of the coatings, thus increasing the hydrophobicity of the coatings. The contact angles of the coatings reached maximum value around the Tg of the polymers. When the assembly temperature was beyond the Tg, the particles softened and fused with each other to produce relatively smoother surface. Thus the hierarchical structures with nanosized corona particles on the surface of submicrosized particles were damaged, which casued reduction of the roughness of the coatings and decreased the apparent hydrophobicity.

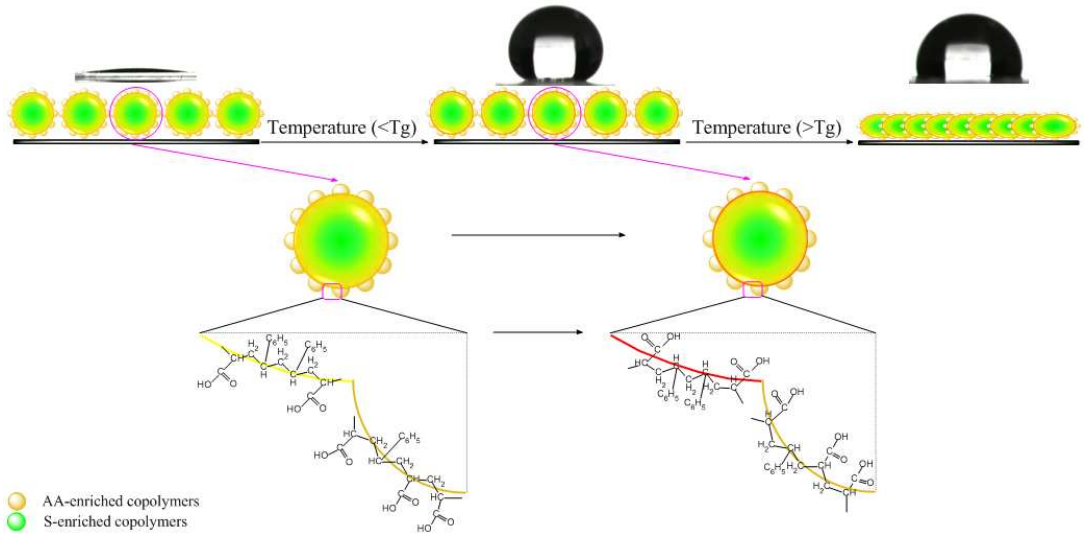

Scheme 1 Schematic illustration of the wettability transition of the coatings assembly from P(S-AA) particle.

4. Conclusion

In conclusion, monodisperse raspberry-like P(S-AA) particles were successfully synthesized using a one-step soap-free emulsion polymerization of S and AA accompanied by phase separation. The formation of raspberry-like particles was caused by phase separation between the S-enriched copolymers obtained in the later stage of the polymerization and the AA-enriched copolymers produced in the early stage of the polymerization. The morphologies and roughness of the raspberry-like particles can be easily tailored by adjusting the amount of S, AA and DVB. Hierarchical structured coatings were assembled by a facile vertical deposition method using the as-prepared raspberry-like particles. The wettability of the coatings could be easily tuned from hydrophilicity to superhydrophobicity by controlling the assembly temperature. The transition of the wettability of the coatings was attributed to a thermodynamic-driven process that hydrophobic groups in the particles migrated toward the surface of the coatings, and a decrease of the surface roughness because of the softening and fusing of the particles at the temperature above the Tg of the polymers. This research provided a convenient approach to fabricate hydrophilic or superhydrophobic coatings by altering the chemical composition and morphologies of the raspberry-like particles and the assembly temperature without any specialized equipments or any additional modifications with low surface energy materials, although the coatings were fragile and the mechanical strength needed to be improved, relative improvement is ongoing in our lab.

Acknowledgements

This work was supported by the National High Technology Research and Development Program of China (863 Program) (Grant No. 2012AA02A404), the Key Program of the National Natural Science Foundation of China (Grant No. 51433008), the General Program of the National Natural Science Foundation of China (Grant No. 51173146) and the Basic Research of Northwestern Polytechnical University (Grant No. 3102014JCQ01094, JC20120248, 3102014ZD).

Notes

[a] Department of Applied Chemistry, School of Science, Northwestern Polytechnical University, Xi'an 710072, PR China

[*] E-mail: qyzhang@nwpu.edu.cn

Electronic Supplementary Information (ESI) available: [Detailed experimental conditions for the preparation of raspberry-like P(S-AA) particles; DLS size distribution and elemental composition of P(S-AA) particles prepared with different experimental conditions; advancing contact angles, receding contact angles and CAH of the coatings assembly from the particles prepared with 60% S and 40% AA assembled at temperatures various from 50 to 120 °C; DSC curve of P(S-AA) raspberry-like particles prepared with 60% S and 40% AA; typical 3-dimensional AFM images of the coatings assembly from the particles prepared with 60% S and 40% AA; Roughness factors of the coatings assembly from particles prepared with 60% S and 40% AA fabricated at different temperatures]. See DOI: 10.1039/b000000x/

REFERENCES

1 Y. Gao, I. Gereige, A. El Labban, D. Cha, T. T. Isimjan and P. M. Beaujuge, *ACS Appl. Mater. Interfaces,* 2014, **6**, 2219-2223.
2 U. Tuvshindorj, A. Yildirim, F. E. Ozturk and M. Bayindir, *ACS Appl. Mater. Interfaces*, 2014, **6**, 9680-9688.
3 H. J. Gwon, Y. Park, C. W. Moon, S. Nahm, S.-J. Yoon, S. Y. Kim and H. W. Jang, *Nano Res.*, 2014, **7**, 670-678.
4 G. D. Bixler and B. Bhushan, *Nanoscale*, 2013, **5**, 7685-7710.
5 C. Lee and C. J. Kim, *Phys. Rev. Lett.*, 2011, **106**.
6 J. A. Callow and M. E. Callow, *Nat. Commun.*, 2011, **2**, 244.
7 J. Genzer and K. Efimenko, *Biofouling*, 2006, **22**, 339-360.
8 H. Zhang, R. Lamb and J. Lewis, *Sci. Technol. Adv. Mater.*, 2005, **6**, 236-239.
9 R. B. Pernites, C. M. Santos, M. Maldonado, R. R. Ponnapati, D. F. Rodrigues and R. C. Advincula, *Chem. Mater.*, 2012, **24**, 870-880.
10 R. Yang, Y. Zhang, J. Li, Q. Han, W. Zhang, C. Lu, Y. Yang, H. Dong and C. Wang, *Nanoscale*, 2013, **5**, 11019-11027.
11 A. Asthana, T. Maitra, R. Buchel, M. K. Tiwari and D. Poulikakos, *ACS Appl. Mater. Interfaces*, 2014, **6**, 8859-8867.
12 B. Li, L. Wu, L. Li, S. Seeger, J. Zhang and A. Wang, *ACS Appl. Mater. Interfaces*, 2014, **6**, 11581-11588.
13 Lei Wu, Junping Zhang, Bucheng Li and A. Wang, *Polym. Chem.*, 2014, **5**, 2382-2390.
14 Y. Yoo, J. B. You, W. Choi and S. G. Im, *Polym. Chem.*, 2013, **4**, 1664.
15 J. Zhang, B. Li, L. Wu and A. Wang, *Chem. Commun.*, 2013, **49**, 11509-11511.
16 J. Zimmermann, F. A. Reifler, G. Fortunato, L. C. Gerhardt and S. Seeger, *Adv. Funct. Mater.*, 2008, **18**, 3662-3669.
17 A. C. Lima, C. A. Custódio, C. Alvarez-Lorenzo and J. F. Mano, *Small*, 2013, **9**, 2487-2492.
18 R. Luo, Y. Cao, P. Shi and C. H. Chen, *Small*, 2014.
19 R. N. Wenzel, *Ind. Eng. Chem.*, 1936, **28**, 988-994.
20 A. Cassie and S. Baxter, *Trans. Faraday Soc.*, 1944, **40**, 546-551.
21 H.-J. Choi, S. Choo, J.-H. Shin, K.-I. Kim and H. Lee, *J. Phys. Chem. C*, 2013, **117**, 24354-24359.
22 S. M. Kang, I. You, W. K. Cho, H. K. Shon, T. G. Lee, I. S. Choi, J. M. Karp and H. Lee, *Angew. Chem. Int. Ed.*, 2010, **49**, 9401-9404.
23 J. Feng, M. T. Tuominen and J. P. Rothstein, *Adv. Funct. Mater.*, 2011, **21**, 3715-3722.
24 X. Deng, L. Mammen, H. J. Butt and D. Vollmer, *Science*, 2012, **335**, 67-70.
25 J. H. Kong, T. H. Kim, J. H. Kim, J. K. Park, D. W. Lee, S. H. Kim and J. M. Kim, *Nanoscale*, 2014, **6**, 1453-1461.
26 C. W. Peng, K. C. Chang, C. J. Weng, M. C. Lai, C. H. Hsu, S. C. Hsu, S. Y. Li, Y. Wei and J. M. Yeh, *Polym. Chem.*, 2013, **4**, 926-932.
27 K. Ellinas, S. P. Pujari, D. A. Dragatogiannis, C. A. Charitidis, A. Tserepi, H. Zuilhof and E. Gogolides, *ACS Appl. Mater. Interfaces*, 2014, **6**, 6510-6524.
28 M. Toma, G. Loget and R. M. Corn, *ACS Appl. Mater. Interfaces*, 2014, **6**, 11110-11117.
29 S. H. Lee, Z. R. Dilworth, E. Hsiao, A. L. Barnette, M. Marino, J. H. Kim, J. G. Kang, T. H. Jung and S. H. Kim, *ACS Appl. Mater. Interfaces*, 2011, **3**, 476-481.
30 A. M. Coclite, Y. Shi and K. K. Gleason, *Adv. Funct. Mater.*, 2012, **22**, 2167-2176.
31 D. Zhu, X. Lu and Q. Lu, *Langmuir*, 2014, **30**, 4671-4677.
32 Y. Song, R. P. Nair, M. Zou and Y. Wang, *Nano Res.*, 2010, **2**, 143-150.
33 A. H. Broderick, U. Manna and D. M. Lynn, *Chem. Mater.*, 2012, **24**, 1786-1795.
34 Y. Li, S. Chen, M. Wu and J. Sun, *Adv. Mater.*, 2014.
35 K. Manabe, S. Nishizawa, K. H. Kyung and S. Shiratori, *ACS Appl. Mater. Interfaces*, 2014, **6**, 13985-13993.

36 X. Du, J. S. Li, L. X. Li and P. A. Levkin, *J. Mater. Chem. A*, 2013, **1**, 1026.
37 Y. Huang, X. Liu, F. Zhang, J. Dong, Y. Luo and C. Huang, *Polym. J.*, 2012, **45**, 125-128.
38 S. Kato and A. Sato, *J. Mater. Chem.*, 2012, **22**, 8613.
39 X. Li, C. Wang, Y. Yang, X. Wang, M. Zhu and B. S. Hsiao, *ACS Appl. Mater. Interfaces*, 2014, **6**, 2423-2430.
40 A. Davis, Y. H. Yeong, A. Steele, I. S. Bayer and E. Loth, *ACS Appl. Mater. Interfaces*, 2014, **6**, 9272-9279.
41 L. Xiong, L. L. Kendrick, H. Heusser, J. C. Webb, B. J. Sparks, J. T. Goetz, W. Guo, C. M. Stafford, M. D. Blanton, S. Nazarenko and D. L. Patton, *ACS Appl. Mater. Interfaces*, 2014, **6**, 10763-10774.
42 B. P. Dyett, A. H. Wu and R. N. Lamb, *ACS Appl. Mater. Interfaces*, 2014, **6**, 9503-9507.
43 R. K. Wang, H. R. Liu and F. W. Wang, *Langmuir*, 2013, **29**, 11440-11448.
44 Y. Wang, W. Huang, L. Huang, S. Zhang, D. Hua and X. Zhu, *Polym. Chem.*, 2013, **4**, 2255-2259.
45 P. Roach, N. J. Shirtcliffe and M. I. Newton, *Soft Matter*, 2008, **4**, 224.
46 Y. Y. Yan, N. Gao and W. Barthlott, *Adv. Colloid. Interface Sci.*, 2011, **169**, 80-105.
47 B. Bhushan and Y. C. Jung, *Prog. Mater. Sci.*, 2011, **56**, 1-108.
48 X. Wang, B. Ding, J. Yu and M. Wang, *Nano Today*, 2011, **6**, 510-530.
49 W. Jiang, C. M. Grozea, Z. Shi and G. Liu, *ACS Appl. Mater. Interfaces*, 2014, **6**, 2629-2638.
50 A. M. Telford, B. S. Hawkett, C. Such and C. Neto, *Chem. Mater.*, 2013, **25**, 3472-3479.
51 A. Milionis, D. Fragouli, L. Martiradonna, G. C. Anyfantis, P. D. Cozzoli, I. S. Bayer and A. Athanassiou, *ACS Appl. Mater. Interfaces*, 2014, **6**, 1036-1043.
52 D. Tulli, S. D. Hart, P. Mazumder, A. Carrilero, L. Tian, K. W. Koch, R. Yongsunthon, G. A. Piech and V. Pruneri, *ACS Appl. Mater. Interfaces*, 2014, **6**, 11198-11203.
53 S. S. Latthe and A. L. Demirel, *Polym. Chem.*, 2013, **4**, 246-249.
54 J. Wang, Y. Wen, X. Feng, Y. Song and L. Jiang, *Macromol. Rapid Commun.*, 2006, **27**, 188-192.
55 J. Wang, Y. Wen, J. Hu, Y. Song and L. Jiang, *Adv. Funct. Mater.*, 2007, **17**, 219-225.
56 X. Fan, X. Jia, H. Zhang, B. Zhang, C. Li and Q. Zhang, *Langmuir*, 2013, **29**, 11730-11741.
57 H. Shirahama and T. Suzawa, *Colloid Polym. Sci.*, 1985, **263**, 141-146.
58 H. Shirahama and T. Suzawa, *Polym. J.*, 1984, **16**, 795-803.
59 P. H. Wang and C. Y. Pan, *Colloid Polym. Sci.*, 2002, **280**, 152-159.
60 D. Polpanich, P. Tangboriboonrat and A. Elaıssari, *Colloid Polym. Sci.*, 2005, **284**, 183-191.
61 K. U. Fulda, A. Kampes, L. Krasemann and B. Tieke, *Thin Solid Films*, 1998, **327-329**, 752-757.
62 E. C. Chapin, G. E. Ham and C. L. Mills, *J. Polym. Sci.*, 1949, **4**, 597-604.
63 G. W. Hastings, *Chem. Commun.* , 1969, **18**, 1039-1039.
64 S. Kamei, M. Okubo and T. Matsumoto, *J. Polym. Sci. Part A: Polym. Chem.*, 1986, **24**, 3109-3116.
65 Y. Sun, Y. Yin, M. Chen, S. Zhou and L. Wu, *Polym. Chem.*, 2013, **4**, 3020-3027.
66 A. S. Dimitrov and K. Nagayama, *Langmuir*, 1996, **12**, 1303-1311.
67 Y. G. Ko and D. H. Shin, *J. Phys. Chem. B*, 2007, **111**, 1545-1551.
68 L. Feng, Y. Zhang, J. Xi, Y. Zhu, N. Wang, F. Xia and L. Jiang, *Langmuir*, 2008, **24**, 4114-4119.
69 A. F. Routh and W. B. Russel, *Langmuir*, 1999, **15**, 7762-7773.
70 A. M. Mathur, B. Drescher, A. B. Scranton and J. Klier, *Nature*, 1998, **392**, 367-370.

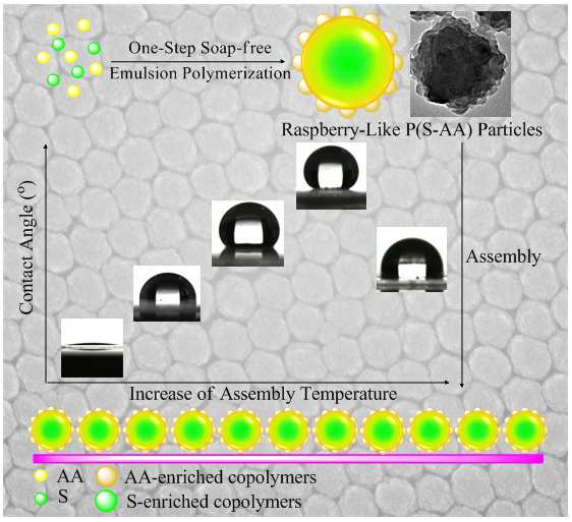

Hierarchical structured coatings with wettability could be tuned from hydrophilicity to superhydrophobicity are fabricated by assembly of raspberry-like P(S-AA) particles